INSAR QUALITY CONTROL: ANALYSIS OF FIVE YEARS OF CORNER REFLECTOR TIME SERIES

Petar Marinkovic, Gini Ketelaar, Freek van Leijen, and Ramon Hanssen

Delft University of Technology, Delft Institute of Earth Observation and Space Systems (DEOS), Kluyverweg 1, 2629HS, Delft, The Netherlands, Email: P.Marinkovic@tudelft.nl

ABSTRACT

A persistent scatterer experiment using corner reflectors has been set up to validate the quality of InSAR Envisat/ERS-2 phase observations. The validation is performed by means of independent precise leveling observations of corner reflector motion in time, and comparison with respect to InSAR observables. The estimated precision of the InSAR double-differenced phase measurements is 2.8mm (vertical) for "zero-gyro" ERS-2 data and 1.6mm for Envisat. An analysis of an integration of corner reflectors and neighboring "natural" persistent scatterers is also presented.

Key words: InSAR; PSI; quality description; corner reflector.

1. INTRODUCTION

Quality control for InSAR and PSI measurements is notoriously difficult, due to the lack of a well-defined effective scattering center, the absence of redundant measurements, and the phase ambiguity estimation problem. Only using a heuristic approach, based on assumptions on ergodicity in space and/or time, it is possible to derive estimates and retrieve quality parameters.

Corner reflectors are the only option to retrieve a well known scattering center, making them very useful for validation purposes. In the Delft Corner Reflector Experiment (DCRE) five corner reflectors have been deployed since early 2003, see Figures 1; oriented towards a descending track of Envisat and ERS-2. During these years, the reflectors have been manually leveled with millimiter precision, to build a strong validation archive. Ground water table measurements have been performed for better interpretation of the results.

The main objective of DCRE is to simulate a set of stable scatterers whose phase history can be validated by additional direct measurements. A period of almost five years was analyzed in order to gather enough statistics to draw conclusions on the quality of the phase time history, and hence InSAR deformation measurements.

2. THE DELFT TEST SITE

2.1. Ancillary Data - Leveling

Shortly before or after each satellite pass, usually within 24hrs, a leveling of the corner reflectors is performed. The leveling network was designed introducing redundant measurements, making it possible to detect outliers and give a quality description of the estimated heights, [6]. The network contains two benchmarks founded on a stable subsurface layer. The height difference between benchmarks points varies at most ± 0.5 mm and can therefore be considered as stable.

Studying the time series of the corner reflector heights with reference to their initial heights, see Figure 2, a seasonal effect (amplitude of 1–2cm) is visible which appears to be superposed on a secular settling effect of the corner reflectors in the soil. Furthermore, since the precision of the leveling heights is in the range of 0.3–1.5mm, this seasonal signal may be detectable by InSAR.

2.1.1. Double–difference observations

Leveling and InSAR observations are inherently not the same, i.e., their spatio-temporal content is different. A leveling measurement is a spatial height difference between two points at a certain time, which can be directly measured. A PSI measurement is a temporal interferometric difference between master and slave observation time, for a certain point. Hence, the first interpretable PSI observation is the double–difference, both temporally (between master and slave acquisition time) and spatially (between

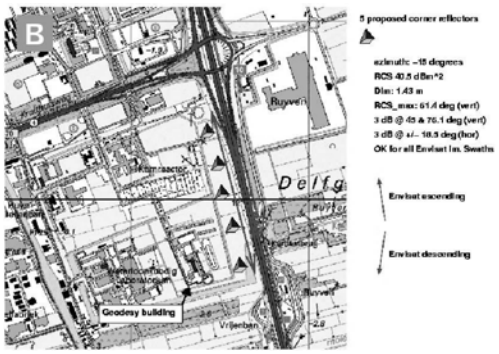

Figure 1. A topographic map of the corner reflector area and details of the radar cross section of the reflectors.

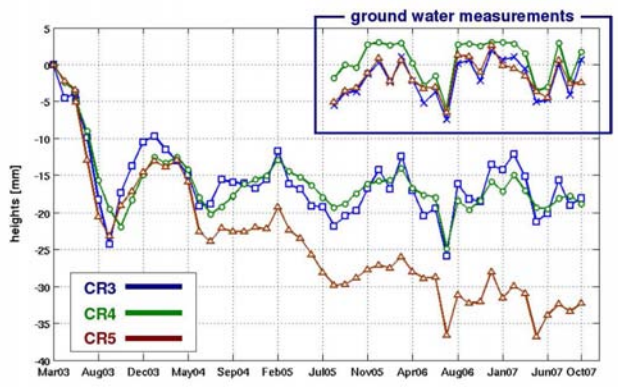

Figure 2. Estimated leveling heights with reference to fixed benchmark for the period March 2003 - October 2007. The seasonal effect has an amplitude of 1–2cm. The seasonal trend is visible - during summer months the corner reflectors subside whereas in autumn an uplift is obvious. Since August 2005 ground–water levels have been measured, which show a high correlation with the seasonal corner reflector displacements. In periods of high precipitation the soil swells, which causes an uplift of the corner reflectors, as they are mounted on a shallow subsurface layer. The vertical axis is relative for the ground water levels. The amplitude is a factor 10 larger then the reflector movement.

two points). Therefore, in order to be able to compare the leveling to InSAR observations they have to be converted to double–differences along the vertical. Since the distance between the corner reflectors is small, in this study differences between orthometric and geometric heights are considered negligible.

2.2. InSAR data

Two data sets were independently analyzed, two stacks of ERS-2 and Envisat data. Both stacks consisted of all available images for the area since the beginning of the experiment (01.03.2003): in total 37 images for ERS-2 and 44 for the Envisat stack.

Note that since 2001, ERS-2 operates in Zero-Gyro mode, which does not guarantee the stability of the satellite orbital attitude as defined in the mission requirements. As consequence the Doppler centroid for repeated acquisitions over a certain area varies continuously.

2.2.1. InSAR observations

With interferometry two radar observations are combined, and consequently the phase of the slant range difference ϕ_x is measured, [1]. Moreover, the wrapped phase ϕ_x^k of a point in differential interferogram k can be decomposed to:

$$\phi_x^k = W\{\phi_{x,\text{topo}}^k + \phi_{x,\text{defo}}^k + \phi_{x,\text{obj}}^k + \phi_{x,\text{atmo}}^k + \phi_{x,\text{orbit}}^k + \phi_{x,\text{noise}}^k\} \quad (1)$$

where $W\{\cdot\}$ is the wrapping operator, ϕ_{topo} is the phase caused by uncompensated topography, ϕ_{defo} is the phase caused by displacement of the target in time between acquisitions, ϕ_{obj} is the object scattering phase related to the path length traveled in the resolution cell, ϕ_{atmo} is the atmospheric phase accounting for signal delays, ϕ_{orbit} is contribution caused by imprecise orbit data, and ϕ_{noise} is the additive noise term.

In the case of controlled experiment like this one, the deformation term is considered to be the only unknown in Eq. (1). The InSAR double–differences are unwrapped to the closest leveling double–difference. The height of the corner reflectors is measured by GPS. As the maximum distance to the reference corner reflector is 200 meters, atmospheric and orbital effects are assumed to be negligible in the spatial differences. The InSAR phase is also corrected for the ϕ_{obj} term, as elaborated on in Appendix A.

3. VALIDATION: A-POSTERIORI PRECISION ESTIMATION, THEORY

This section reviews the theoretical setup for the a-posteriori precision estimation of InSAR double–differences utilizing Variance Component Estimation (VCE). The procedure is based on the comparison of independent leveling and InSAR measurements. A mathematical model is set up that consists of a functional and a stochastic model. The functional model describes the relation between the leveling and InSAR observations. The stochastic model represents the precision of both measurement techniques.

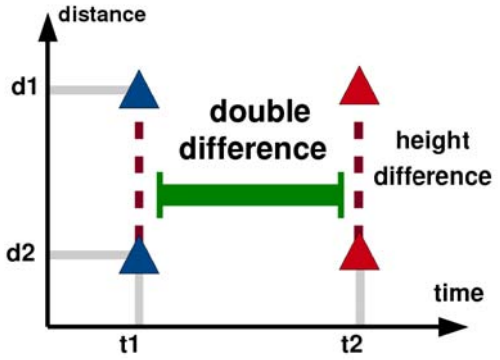

Figure 3. Leveling double–differences: "first in space then in time".

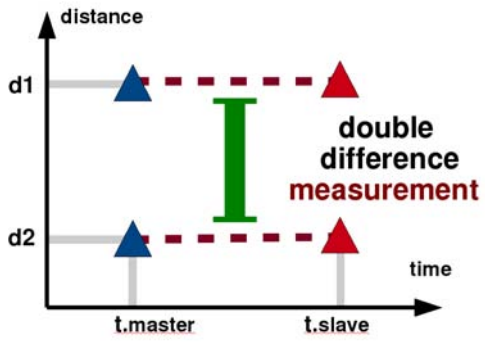

Figure 4. InSAR/PSI double–differences: "first in time then in space".

3.1. Functional model

The functional model consists of independent condition equations, [6]. The reasoning underlying the condition equations states that the leveling double–differences should be equal to the InSAR double–differences:

$$B^T E\{\underline{y}\} = \begin{bmatrix} -I & I & 0 \\ -I & 0 & I \end{bmatrix} E\{ \begin{bmatrix} \underline{d}_{\rm lev} \\ \underline{d}_{\rm ERS} \\ \underline{d}_{\rm EV} \end{bmatrix} \} = 0, \qquad (2)$$

where:

B	condition equation design matrix,
$\underline{y}$	vector of observables,
I	identity matrix,
$\underline{d}_{\rm lev}$	leveling double–differences (mm, vertical),
$\underline{d}_{\rm ERS}$	ERS double–differences (mm,vertical),
$\underline{d}_{\rm EV}$	Envisat double–differences (mm,vertical).

3.2. Stochastic model

The stochastic model, that is represented by the variance-covariance matrix, describes the precision of the leveling and InSAR double–difference observations. Leveling, ERS and Envisat observations are independent. However, double–differences from a single technique are mutually dependent. Hence, the variance-covariance matrix Q_y corresponding with the system of condition equations has a block-diagonal shape:

$$Q_y = \begin{bmatrix} \sigma^2_{\rm lev} Q_{\rm lev} & 0 & 0 \\ 0 & \sigma^2_{\rm ERS} Q_{\rm ERS} & 0 \\ 0 & 0 & \sigma^2_{\rm EV} Q_{\rm EV} \end{bmatrix}. \qquad (3)$$

The variance-covariance matrix of the InSAR double–differences is based on the Signal-to-Clutter ratio of the single SLC phases, converted to mm along the vertical. The propagation law of variances and covariances has been applied to obtain the full variance-covariance matrix, [2].

3.3. A-posteriori precision estimation

The a-posteriori precision estimation for InSAR and leveling double–differences is performed applying Variance Component Estimation [5]. The leveling observations have been obtained in a redundant measurement network. Per epoch, a testing procedure has been performed, followed by the estimation of one variance factor. Hence, the precision and reliability of the leveling double–differences are well established. Therefore, the variance-covariance matrix is split into a known (leveling) and an unknown (InSAR) part prior to VCE:

$$Q_y = Q_0 + \sum_{k=1}^{2} \sigma_k^2 Q_k, \qquad (4)$$

where Q_0 is the cofactor matrix of the leveling double–differences, and Q_k are the cofactor matrices of the InSAR double–differences. Two variance factors σ_k^2 are estimated: one for ERS and one for Envisat.

4. VALIDATION: RESULTS

This section reviews the results of a comparison of double–difference leveling and InSAR measurements. Results of the precision of InSAR measurements, derived following the mathematical framework presented in Section 3, are also presented. Moreover, a performance in terms of the InSAR double–difference standard deviation, of different corrections, i.e., sub-pixel and Doppler annotation correction is also given.

The analysis strategy was to start with a "raw" (i.e., no corrections nor outlier removal) InSAR and leveling data comparison, and then to systematically apply corrections, and remove possible outliers in InSAR data, by monitoring the improvement of the standard deviation of InSAR double–differenced phase. The applied sub–pixel corrections are summarized in Appendix A.

The main results of the analysis are visualized in Figures 5, 6, 7. In all figures, double–differences of leveling are graphically compared to InSAR double–differences; namely reflectors 3 (bottom) and 5 (top) relative to reflector 4. ERS-2 results are illustrated by a red line, and Envisat with a blue one. The leveling time series is visualized with a gray stripe, indicating a range of $\pm$1.5mm standard deviation around the measurements.

Finally, Tables 1 and 2 summarize the a-posteriori precision of InSAR double–differences, converted to the vertical, for all analysis performed.

1σ : NO OUTLIER REMOVAL		
corrections applied:	**ERS-2**	**ASAR**
no corrections	10.7mm	2.4mm
sub-pixel correction	6.9mm	1.7mm
sub-pixel and fDC correction	4.1mm	1.7mm

Table 1. Summary of a-posteriori estimated precision of InSAR double–difference phase observations for different observation/experiment strategies: NO OUTLIER REMOVAL case

1σ : WITH OUTLIER REMOVAL		
corrections applied:	**ERS-2**	**ASAR**
no corrections	4.5mm	2.4mm
sub-pixel correction	2.9mm	1.6mm
sub-pixel and fDC correction	2.8mm	1.6mm

Table 2. Summary of a-posteriori estimated precision of InSAR double difference phase observations for different observation/experiment strategies: WITH OUTLIER REMOVAL case

4.1. Ambiguities in annotated Doppler centroid information

Studying Figure 6, a bias in results of CR4-CR3 leveling – ERS-2 InSAR comparison is obvious. A possible explanation for this bias could be found by plotting the dependence between the InSAR–leveling differences as a function of Doppler centroid frequencies of stacked ERS-2 images.

A hypothesis is that the difference between ERS-2 InSAR

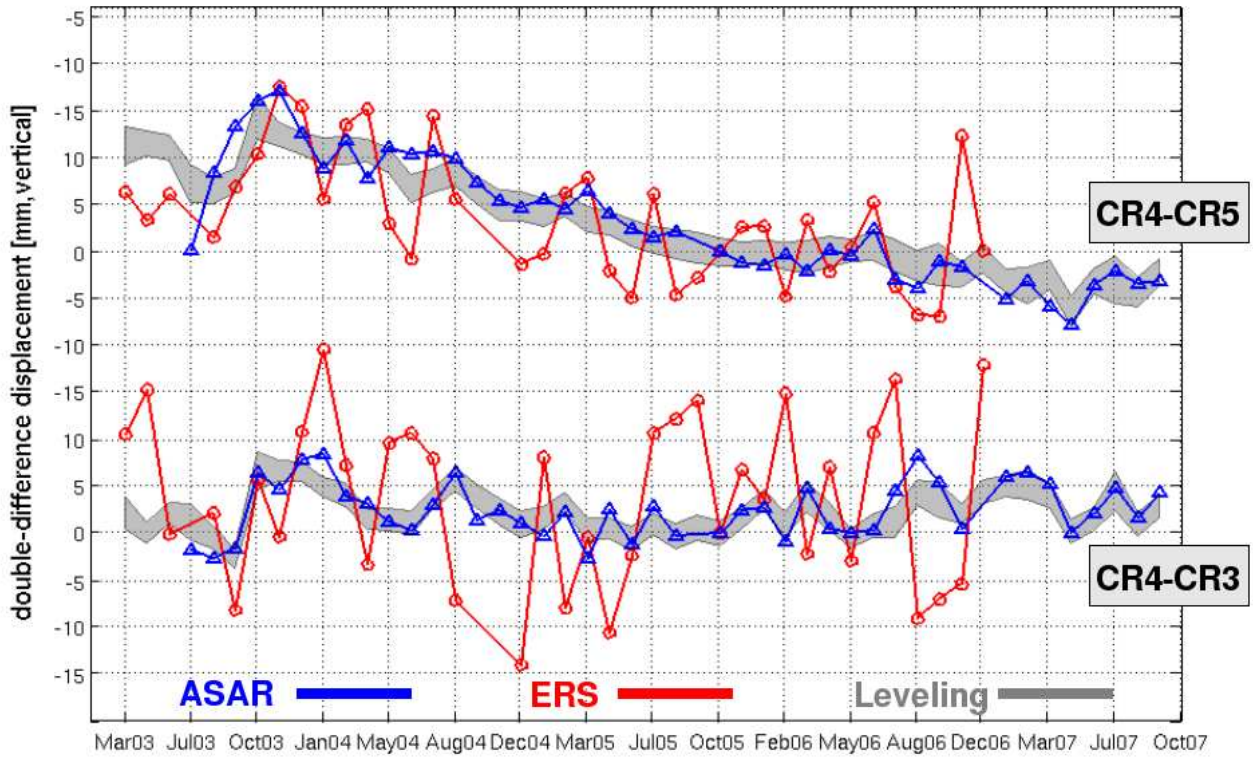

Figure 5. Time history of InSAR double differences, before sub–pixel correction, compared to leveling double differences. A gray stripe indicates a range of ±1.5 mm of standard deviation of leveling measurements. The estimated standard deviation of double–difference InSAR phase in this case are 10.7mm (vertical) for ERS-2 while 2.4mm (vertical) for Envisat.

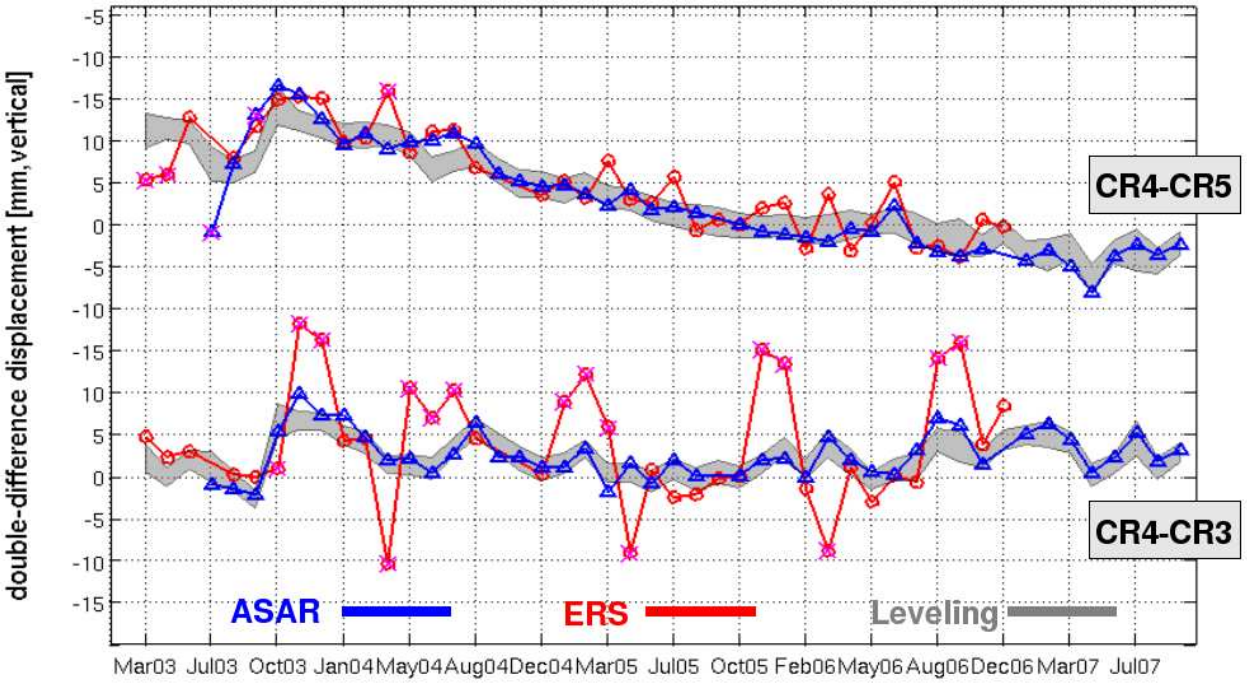

Figure 6. The visualized results are corrected with sub-pixel correction, that compensate for viewing geometry differences (see Appendix A). Observations considered as outliers are marked with red crosses. The systematic behavior of outliers of CR4–CR3 results triggered an in-detail study of the Doppler centroid frequency annotated in the ERS data products, see 4.1. In this case, estimated the standard deviation of double–difference InSAR phase are 2.9mm (vertical) for ERS-2 while 1.6mm (vertical) for Envisat.

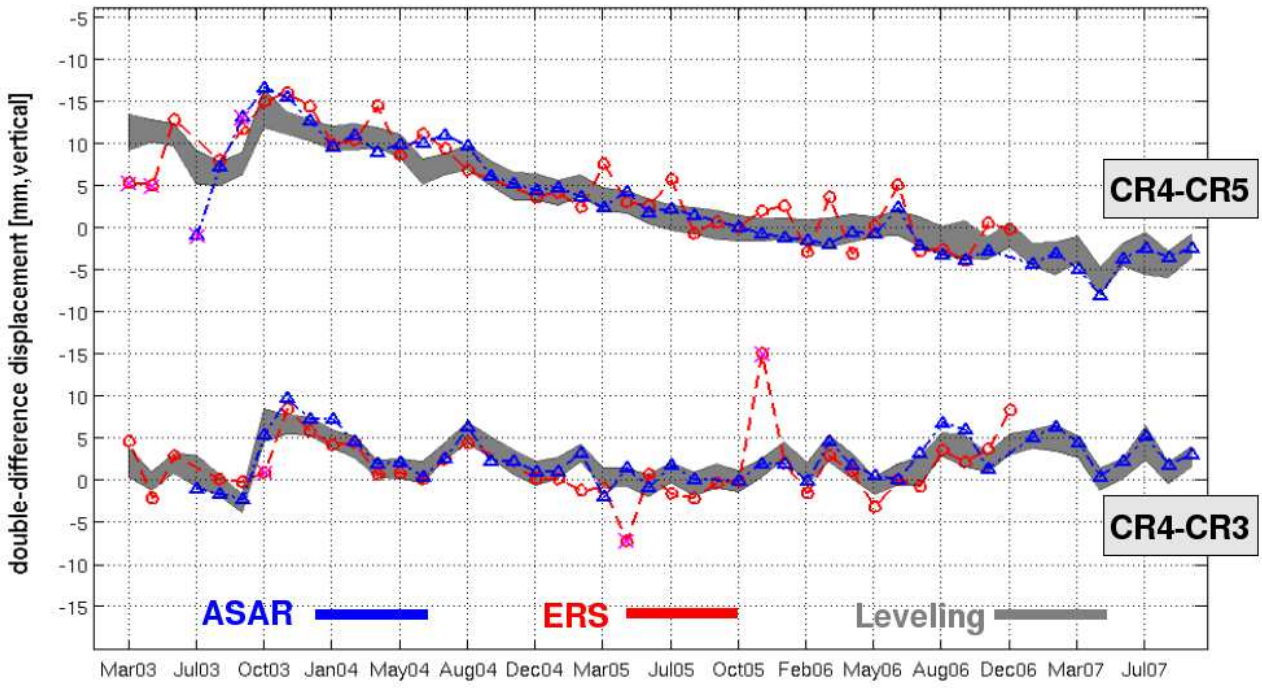

Figure 7. The sub-pixel correction to compensate for viewing geometry differences is applied, and in ERS-2 case the correction for possible ambiguities in annotation of fDC is also utilized (see Section 4.1). Outlier removal was also performed, as indicated by red crosses. The estimated standard deviation of double–difference InSAR phase are 2.8mm (vertical) for ERS-2, while 1.6mm (vertical) for Envisat. Note that the standard deviation of double–differenced InSAR phase is in the same order, as with values obtained with no correction for Doppler ambiguities, while number of outliers in ERS-2 time series is being reduced for approximately 80%. Hence, the correction for Doppler ambiguities does not introduce any additional smoothing nor "artificial" results improvement.

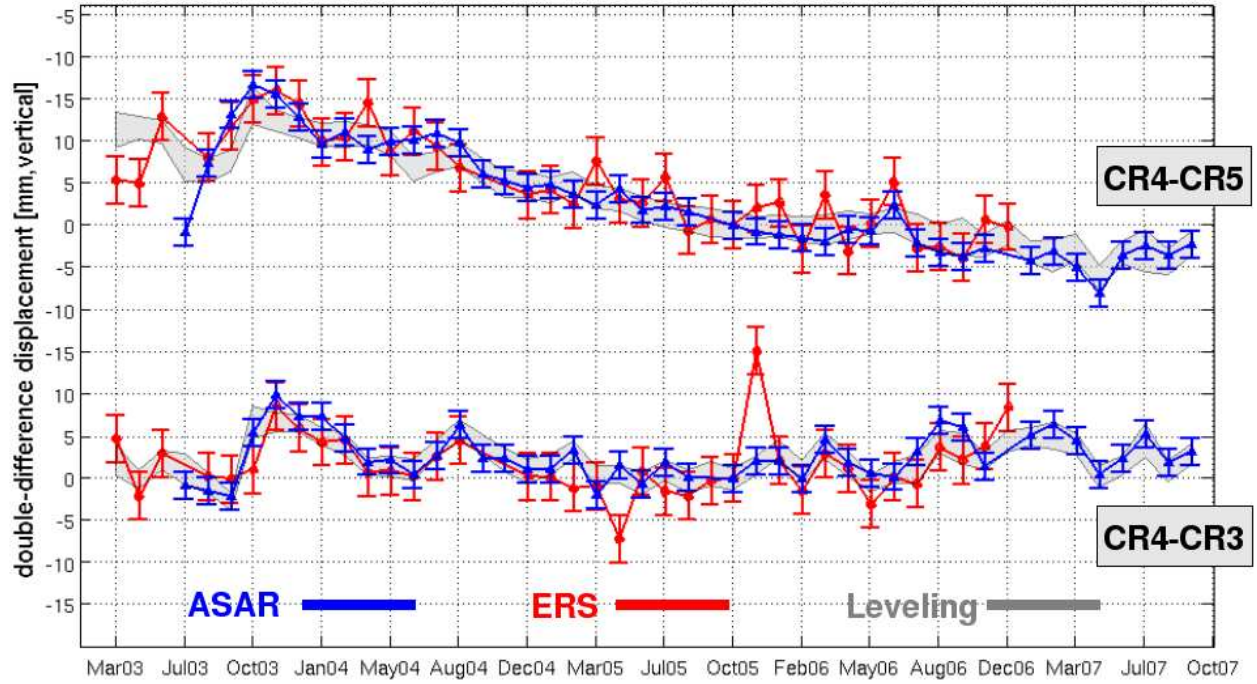

Figure 8. Visualization of empirically derived error bars of InSAR double–differences. The error bars represent the precision of each measurement technique between "1-σ" criterion. The results show that the measurement techniques, i.e. leveling and InSAR, are in the agreement within the error bounds. This plot can be also considered as a conclusion of this study.

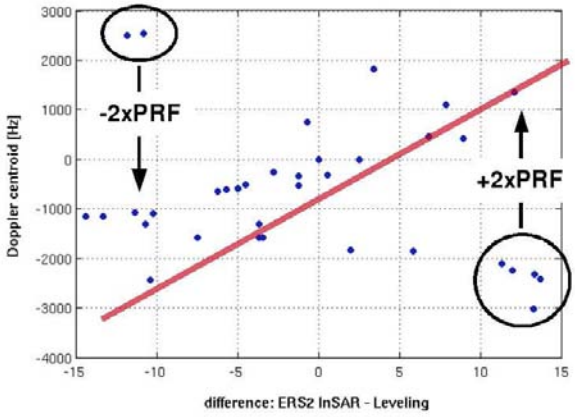

Figure 9. A scatter plot of ERS-2 InSAR – leveling differences as a function of Doppler centroid frequency of stacked ERS-2 images. The blue circles indicate an ambiguity in annotated Doppler centroid frequency values.

results and leveling is a function of Doppler centroid frequency. Hence, as a Doppler frequency difference deviates from zero value, the observed leveling – InSAR difference should increase/decrease. However, analysis of Figure 9, indicates that for the majority of differences the hypothesis is confirmed. However, for few observations, again, the systematic offset is present. Correcting these Doppler centroid frequency values, as indicated by circles on Figure 9, for multiples of the Pulse Repetition Frequency to fit the red line and recomputing the sub-pixel correction in azimuth for these observation leads to significantly improved results, as argued in Figure 7.

4.2. Outlier removal: discussion

Disregarding unmodeled systematic effects in the analysis, such as sub–pixel correction, could result in significant deviations from the leveling measurements. See Figure 5, and refer to values for the standard deviations of InSAR double difference in "no corrections" rows of Tables 1 and 2. These deviations, represent model imperfections. Hence, the model should be adapted instead of the outlier removal. In this case, the initial model adaption is realized with the sub–pixel correction.

However, even after the sub–pixel correction is applied, the outliers in the time series plots are obvious, e.g., see ERS-2 time series depicted in Figure 6. As shown, these deviations can be related to the ambiguities in the annotation of the Doppler centroid frequency values in ERS-2 products. These deviations can be also understood as model imperfections, and subsequently modeled and corrected for.

Moreover, even after modeling and correcting for all the systematic effects, see Figure 7, few outliers in both ERS-2 and Envisat time series are present. It could be argued that in a controlled experiment like this one, outliers, if any, should not be removed. However, the observations of each measurement technique are stochastic. Hence, there is a certain likelihood that outliers would occur. In this context it is justified to remove remaining deviating observations that cannot be addressed to model imperfections.

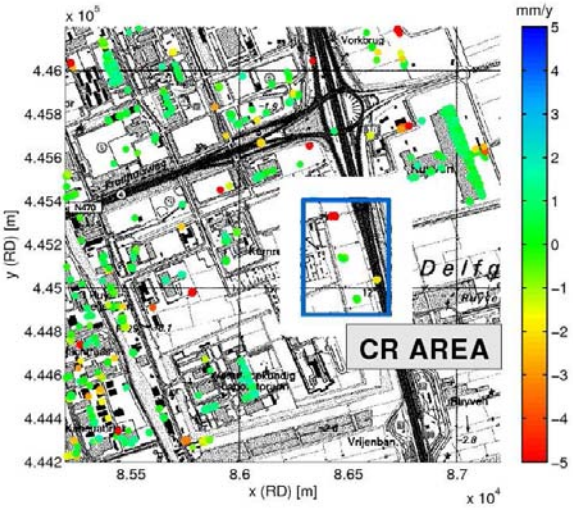

Figure 10. Linear velocities in the corner reflectors area. The standard Delft PSI processing chain was applied.

A possible physical explanation for these outliers could be a presence of water in the reflectors at the time of the acquisition. The most of the outliers are at the beginning of the experiment (early–mid 2003), when the drainage wholes in the reflectors were not big enough; while the later ones are coinciding with extremely rainy acquisition dates.

5. CONNECTION TO THE NATURAL PS

Apart from the direct analysis of the phase behavior of the corner reflectors, and overall PSI analysis is performed for the area of interest. The Delft PSI algorithm was applied on the stack of Envisat images of the city of Delft, and both linear velocities, and periodic signal were estimated, [7]. Figures 10 and 11 visualize the results of the PSI analysis. A direct comparison of leveling, PSI and InSAR point target analysis was also performed. As shown on Figure 12, a comparison of time histories of leveling and PSI estimated

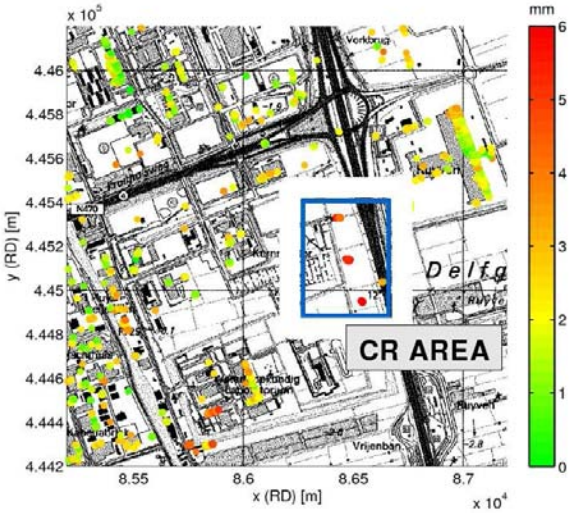

Figure 11. Visualization of the amplitude of the periodic signal, estimated through the joint estimation of the linear velocities and periodic signal.

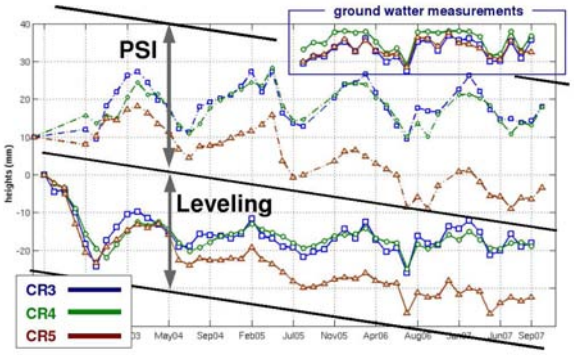

Figure 12. Comparison of time histories of PSI estimated (periodic) deformation and levelling. Note that PSI results are referenced to the arbitrary reference PS that is considered to be stable and not influenced by seasonal effects.

deformations shows that overall deformation trend is well described by PSI measurements. Moreover, a graphical comparison of double differences of InSAR, PSI and leveling observations is also given in Figure 13. Except for one blunder observation in CR4–CR5 time series (most likely as a result of unwrapping error) the correlation between InSAR point target analysis and PSI estimated deformation is on average higher then 95%.

6. CONCLUSIONS

The a-posteriori precision of InSAR double–differenced observations was estimated. In a best case scenario, applying all the listed corrections, the 1σ of Envisat InSAR double–differences is 1.6 mm (vertical), while for "zero-gyro" ERS-2 data it is 2.6 mm (vertical), see Figure 8. Additionally, an in-detail study of the annotated Doppler centroid frequencies values in the ERS data product suggested a possible ambiguities in the parameters annotation.

The results show that the measurement techniques, i.e. leveling and InSAR, are in the agreement within the error bounds. It should be also noted, that the precision of Envisat double–differences is at the level as of the leveling technique applied in this experiment.

Moreover, the corner reflectors are integrated in the PSI analysis. The obtained PSI displacement time series supports the results of the validation experiment.

APPENDIX A: INFLUENCE OF VIEWING GEOMETRY

This correction originally introduced for cross-interferometry, [8], corrects for the systematic phase offsets, depending on the object position (e.g. PS) inside the resolution cell. The practical interpretation of the term would be that it corrects for the "un-compensated" reference phase. As the reference phase is operationally calculated at the "upper left corner" (i.e., leading edges) of a pixel and not at the exact sub-pixel position of the PS point. Hence, this term corrects the interferometric phase as it would be computed at the phase center of the point scatterer (i.e., at the sub-pixel location).

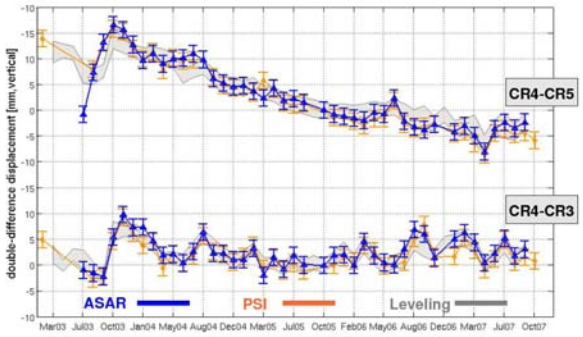

Figure 13. Time history of double differences of PSI, InSAR and leveling. Corner reflector 4 used as reference. The correlation coefficient between deformation estimates obtained by InSAR and PSI is on average higher then 95%. The error bars of InSAR double–difference empirically estimated, showing that all measurement techniques are in agreement withing the error bounds.

A.1 Sub-pixel correction in azimuth

Using a simplified relation to the squint angle ϑ, [1], the azimuth term can be expressed as a function of Doppler centroid frequency:

$$f_{\mathrm{DC}}^{k} \approx \frac{-2v}{\lambda} \sin \vartheta^{k}. \tag{5}$$

where v is the local satellite velocity in an earth-fixed coordinate system. From Figure 14 follows that the additional range to the actual phase center with respect to its starting bin is:

$$\xi_x^k = \xi_x \sin \vartheta^k \tag{6}$$

Substituting Eq. (5) in Eq. (6) follows

$$\xi_x^k = \frac{\lambda}{-2v} f_{\xi_x,\mathrm{DC}}^{k} \cdot \xi_x, \tag{7}$$

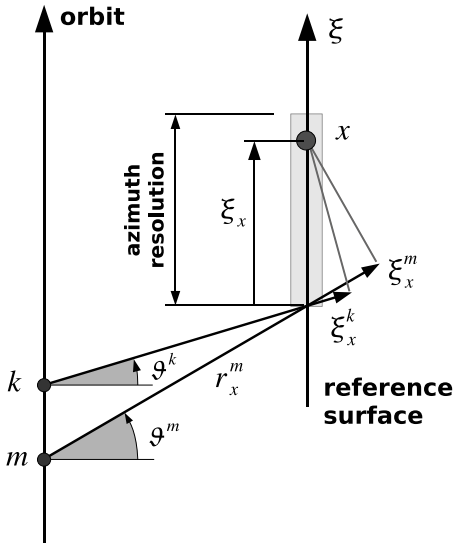

Figure 14. Geometry for a point target located at a sub-pixel position in azimuth.

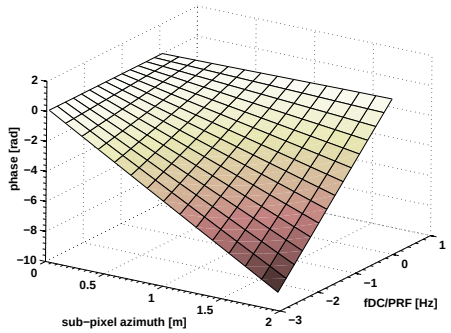

Figure 15. Systematic phase offset in the azimuth direction as a function of scatterer location and Δf_{DC}.

using the ratio $\phi/(2\pi) = -2r/\lambda$, the term Eq. (7) derives to an equivalent of the additional phase of

$$\phi^k_{\xi_x} = \frac{2\pi}{f^k_{x,\mathrm{DC}}} \cdot \xi_x, \tag{8}$$

Note that if sensors are the same the additional phase is independent of the wavelength. Finally, assuming equal sensor velocities υ, the interferometric phase sub-pixel correction for the object location in azimuth direction reads:

$$\phi^{k,m}_{\xi_x} = \frac{2\pi}{\upsilon} \left(f^m_{x,\mathrm{DC}} - f^k_{x,\mathrm{DC}} \right) \cdot \xi_x, \tag{9}$$

A.2 Sub-pixel correction in range

In [4], the interferometric phase introduced by the range sub-pixel location is expressed as:

$$\phi^{k,m}_{\eta_x} = \frac{4\pi}{c} \left(\eta^m_x \Delta_f + \eta^m_x \frac{f^m B_\perp}{r^m \tan\theta^m} \right) \tag{10}$$

where c is the speed of light, f^m is the radar frequency of the master sensor, $\Delta f = f^k - f^m$ is the frequency offset of the slave sensor, η^m_x is the slant-range sub-pixel position, and $B_\perp$ is perpendicular baseline. Using relation $\lambda = c/f$, Eq. (10) can be rewritten in terms of wavelength:

$$\phi_{\eta_x} \approx (\frac{4\pi}{\lambda_k} - \frac{4\pi}{\lambda_m}) \cdot \eta^m_x + \frac{4\pi}{\lambda_k} \frac{B_\perp}{r^m} \cos\theta^m \cdot \eta_x \tag{11}$$

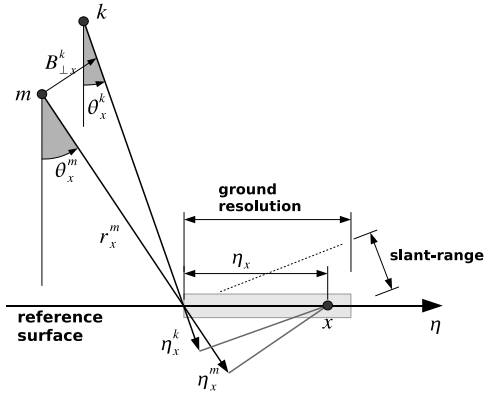

Figure 16. Geometry for a point target located at a sub-pixel position in range.

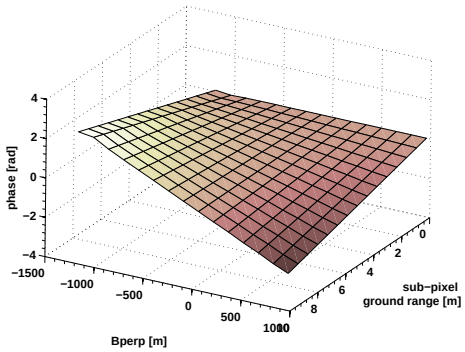

Figure 17. Systematic phase offset in the range direction as a function of scatterer location and perpendicular baseline.

Note that if the wavelength of master and slave carriers are the same, $\lambda^m = \lambda^k = \lambda$, the first term cancels out, while the second term is related to the differences in the viewing geometries, [3] and [4].

ACKNOWLEDGMENTS

We are grateful to European Space Agency for their support of this research through CAT1-1212 project.

REFERENCES

[1] R. Hanssen: *Radar Interferometry: Data Interpretation and Error Analysis*. Kluwer Academic Publishers, 2001.

[2] R. Hanssen: *Stochastic modeling of time series radar interferometry*, in *International Geoscience and Remote Sensing Symposium, Anchorage, Alaska, 20–24 September 2004*, 2004, pp. cdrom, 4 pages.

[3] B.M. Kampes. *Displacement Parameter Estimation using Permanent Scatterer Interferometry*. PhD Thesis, Delft University of Technology, September 2005.

[4] D. Perissin, C. Prati, M. Engdahl, and Y.L. Desnos: Validating the SAR wave-number shift principle with ERS-Envisat PS coherent combination. In *IEEE Transactions on Geoscience and Remote Sensing*, vol. 44, 9:2343–2351, September 2006.

[5] P.J.G. Teunissen: *Towards a Least-Squares Framework for Adjusting and Testing of both Functional and Stochastic Models* Mathematical Geodesy and Positioning Series, volume 26, Delft University Press, 1988.

[6] ——-: *Adjustment theory; an introduction, 1st ed.* Delft: Delft University Press, 2000.

[7] F. van Leijen, and R. Hanssen. Ground water management and its consequences in Delft, the Netherlands as observed by Persistent Scatterer Interferometry. In *Fifth International Workshop on ERS/Envisat SAR Interferometry, 'FRINGE07', Frascati, Italy, 26-30 Nov 2007*.

[8] A. Arnaud, J. Closa, R. Hanssen, N. Adam, M. Eineder, J. Inglada, G. Fitoussi, and B. Kampes: *Development of algorithms for the Exploitation of ERS-Envisat using the Stable Points Network*. ESA Study Contract report, Contract Nr. 16702/02/I-LG, 2004.